GEORISK
https://doi.org/10.1080/17499518.2026.2690494

Taylor & Francis
by informa

OPEN ACCESS Check for updates

Vulnerability model for cantilever retaining walls subject to scour

Lanting Wei[a], Alessandro Tarantino[a], Enrico Tubaldi[a], Hamed Moghaddasi[a] and Daniele Zonta[b]

[a]Department of Civil and Environmental Engineering, University of Strathclyde, Glasgow, UK; [b]Department of Civil, Environmental and Mechanical Engineering, University of Trento, Trento, Italy

ABSTRACT

Retaining walls are widely used to stabilise slopes and support infrastructure such as bridge abutments, culverts, and roads over or adjacent to waterways. These structures can be susceptible to scour-induced erosion and undermining at their toe, which can lead to significant damage and collapse. This paper presents a comprehensive yet simplified analytical formulation to evaluate the reduction in retaining wall capacity caused by scour. First, a model is proposed to describe the scour process at retaining walls. Based on this model, the degradation of retaining wall capacity is formulated by considering various potential failure modes. The proposed formulation, validated against numerical simulations using PLAXIS, is non-dimensionalised to derive simple expressions for describing the effect of scour across different wall geometries, soil properties, and water depths. A simplified approach is then introduced to estimate the scour vulnerability of retaining walls, expressing the conditional probability of wall failure with increasing scour levels. The study provides a practical tool for engineers and infrastructure asset managers to support rapid risk prioritisation of retaining walls exposed to scour, highlighting the most critical parameters influencing the vulnerability of these structures.

ARTICLE HISTORY
Received 12 October 2025
Accepted 10 June 2026

KEYWORDS
Scour; vulnerability; retaining walls; closed-form solution; flooding

1. Introduction

Retaining walls are commonly employed to stabilise slopes and support transport infrastructure elements such as bridge abutments, culverts, and roads over or adjacent to waterways. These structures are susceptible to scour-induced erosion and toe undermining, which can lead to significant damage and structural failure (Khosronejad et al. 2020). Scour at the base of retaining walls is typically associated with four mechanisms: (i) general scour, resulting from the natural evolution of waterways that lowers the elevation of river channels; (ii) constriction scour, where a reduction in river width increases flow velocity within the channel; (iii) local scour, which occurs at the leading edge of retaining walls due to high-energy turbulence and (iv) bend scour, which affects retaining walls along outer banks of meandering rivers due to sudden changes in flow velocity and direction at bends. The interaction of these scour mechanisms can significantly increase the risk of retaining wall failure (Heydari and Diplas 2020). This risk can also be significantly exacerbated by the ageing of these structures and the intensification of extreme weather events and floods due to climate change.

While the vulnerability of bridges to scour has been extensively investigated (Argyroudis and Mitoulis 2021; Scozzese, Tubaldi, and Dall'Asta 2023 Tubaldi et al. 2022;), research on the vulnerability of retaining walls remains limited. Guidelines and standards on scour risk assessment, such as CIRA manuals SP171 and C742 (Kitchen et al. 2021; Kirby et al. 2015), CS 469 (NationalHighways 2024) and French guidelines (Cerema 2019), provide limited information on the evaluation of the scour risk of retaining walls. Furthermore, scour is frequently overlooked in the design of retaining walls located adjacent to watercourses, a practice that has been associated with catastrophic failures (McKelvey 2011). Thus, there is a need to develop scour vulnerability and risk assessment procedures accounting for the specific features of these structures.

The hydraulic processes responsible for scour at the base of longitudinal training walls differ from those acting on bridge piers. A key distinction is that, along retaining walls, lateral flow typically generates elongated scour patterns, whereas pier scour is dominated by downflow and the formation of a horseshoe vortex at the upstream face. Some studies have examined the hydraulic aspects of the problem, especially the evaluation of the scour depth along walls (Heydari and Diplas 2020). Different approaches have been proposed for

CONTACT Enrico Tubaldi enrico.tubaldi@strath.ac.uk Civil and Environmental Engineering, 16 Richmond Street, Glasgow, G1 1XQ, Scotland, UK

© 2026 The Author(s). Published by Informa UK Limited, trading as Taylor & Francis Group
This is an Open Access article distributed under the terms of the Creative Commons Attribution-NonCommercial-NoDerivatives License (http://creativecommons.org/licenses/by-nc-nd/4.0/), which permits non-commercial re-use, distribution, and reproduction in any medium, provided the original work is properly cited, and is not altered, transformed, or built upon in any way. The terms on which this article has been published allow the posting of the Accepted Manuscript in a repository by the author(s) or with their consent.

estimating the scour depth in longitudinal structures through experimental flume studies and empirical formulations (Cely Calixto, Galvis Castaño, and Carrillo Soto 2023; Fael et al. 2006; Khosronejad et al. 2020; Sotiropoulos and Diplas 2017). It has been found that the development of a scour hole is influenced by a wide range of hydraulic, geotechnical factors and geometry of the problem, including the wall's orientation relative to the approaching flow, local flow velocity and turbulence intensity, sediment transport capacity, and the properties of the riverbed material (Cely Calixto, Galvis Castaño, and Carrillo Soto 2023; Sotiropoulos and Diplas 2017). Other studies, discussed in Huang (2017), have investigated the failure mechanisms for reinforced retaining walls under toe scouring action, with a primary emphasis on coastal settings. However, despite the efforts made to understand the hydraulic processes and evaluate the scour depth along retaining walls, the influence of scour on the stability of retaining walls has not received sufficient attention. To the best of the author's knowledge, no previous studies have explicitly proposed models to describe the scour vulnerability of these structures.

The evaluation of the impact of scour on the capacity of retaining walls is a complex task, which must consider the likelihood of occurrence of several failure modes, namely the exceedance of the foundation bearing capacity, the sliding at the base of the foundation and the structure overturning (Theinat et al. 2024). The geometry of the walls, the properties (e.g. friction angle and cohesion) of the backfill and base soil, as well as the water level, all play an important role in the vulnerability assessment and affect both the demand and the capacity. Although advanced numerical models can be developed for investigating the vulnerability of retaining walls, there is a need for vulnerability models which are simple enough to be embedded in standards and used for identifying those walls that are more vulnerable to scour.

This study illustrates a simple yet accurate analytical formulation for evaluating the effect of scour on the safety factor of retaining walls. The proposed formulation uses Lancellotta's earth pressure coefficients to calculate active and passive thrusts (Lancellotta 2002) accounting for wall friction and the bearing capacity model of Hansen and Vesić (Hansen 1970; Vesić 1973), with both models further extended to consider the effect of scour. Validated against the results of advanced numerical analysis of retaining walls in PLAXIS (PLAXIS 2020), the proposed formulation accounts for the various possible limit states that could result in wall failure due to scour.

The analytical formulation is non-dimensionalised, and global sensitivity analysis is performed with the aim of deriving a simple curve that describes the reduction in the partial safety factor with increasing scour levels, accounting for wall geometry, soil properties and water height. The proposed curve can be used for the preliminary assessment of retaining walls and the identification of the most critical parameters that control the wall's safety. In the last part of the paper, fragility functions are developed to describe the conditional probability of wall failure with increasing scour levels.

The rest of the paper is organised as follows. A description of the various actions, resisting mechanisms and limit state functions that underpin the proposed closed-form formulation for the evaluation of the impact of scour on the safety of retaining walls is provided first. Following this, the validation of the formulation is presented, using advanced numerical models developed in PLAXIS (PLAXIS 2020) for three case studies. Next, the paper introduces the non-dimensional formulation that describes the reduction in safety of retaining walls with increasing levels of normalised scour depth, along with the results from global sensitivity analyses that highlight the influence of model parameters on the non-dimensional outcomes. The development of simplified fragility functions for retaining walls exposed to scour is then presented, followed by a conclusion section.

2. Actions and resisting mechanisms for retaining walls exposed to scour

2.1. Problem geometry

Figure 1 illustrates the geometry of the idealised model used to represent both cantilever and gravity retaining walls.

The wall has a total height H, and a foundation width of B, which is made up of the toe length B_t and the heel length B_h. The wall is embedded into the riverbed, with D_F representing the depth from the riverbed surface to the base of the foundation. The water height H_w refers to the vertical distance from the riverbed to the water surface.

Scour is assumed to progress in two stages: first, the riverbed soil is eroded uniformly (Figure 1(b)) until the base of the foundation is reached and the toe is fully exposed. Then, the soil at the base of the foundation is undermined, from the edge of the toe towards the heel, as illustrated in Figure 1(c). The maximum depth of scour below the riverbed is denoted as D_T. During the first stage (i.e. $D_T \leq D_F$ in Figure 1(b)), increasing levels of scour correspond to a reduction of the embedded depth:

$$D_F^{'} = \max(0,\ D_F - D_T) \tag{1}$$

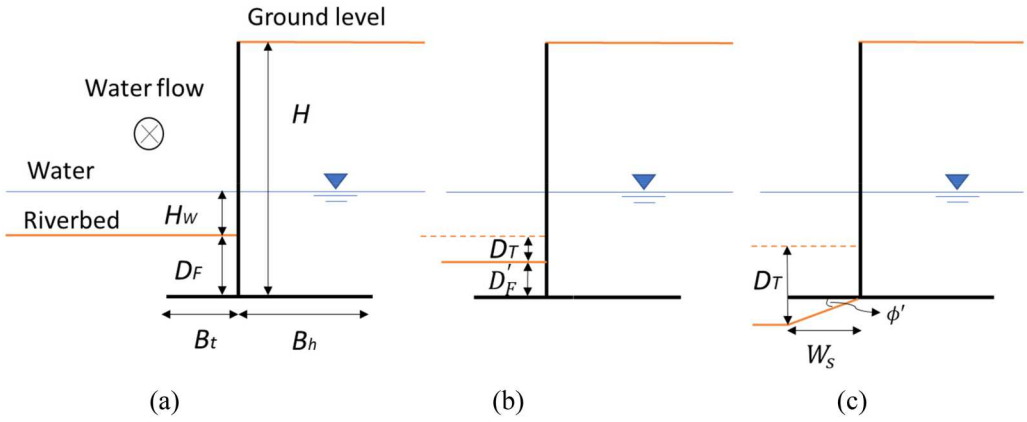

Figure 1. Idealised model of the retaining wall: (a) case of no scour, (b) scour in stage 1: $D_T \leq D_F$, (c) scour in stage 2: $D_T > D_F$

During the second stage (i.e. $D_T > D_F$ in Figure 1(c)), scour undermines the bottom of the foundation and progresses horizontally from the toe to the heel, with a width W_s defined by Equation (2).

$$W_s = \frac{D_T - D_F}{tan\phi'} \tag{2}$$

where the angle of inclination of the scour hole is assumed equal to the effective soil friction angle ϕ'. This assumption idealises the scour slope as being controlled only by riverbed material properties. In reality, scour slope angles are also influenced by other factors, including wall angles relative to the approach flow, flow velocity and turbulence, sediment transport capacity and time-dependent scour development (Cely Calixto, Galvis Castaño, and Carrillo Soto 2023; Sotiropoulos and Diplas 2017). The adopted scour angle is, therefore, intended as a simplified representation for modelling purposes and should be interpreted within the limitations of this assumption.

Figure 2 illustrates actions and resisting mechanisms for retaining walls exposed to scour. The wall is subjected to the active thrust S_a at the edge of the heel and the passive thrust S_p at the edge of the toe. The soil exerts a gravity force W_h and W_t on the heel and toe, respectively. As a result of these actions, the base is subject to a total vertical force N and a total horizontal force T. The total vertical force N is applied with an eccentricity e, measured from the centre of the effective foundation width B'- the portion of the base still in contact with the soil after scour. The maximum horizontal force T_{lim} and the maximum vertical force Q_{lim}, acting beneath the wall base, represent the thresholds beyond which sliding and bearing capacity failures are initiated, respectively.

Failure of retaining walls can occur through three mechanisms. Bearing capacity failure occurs when the

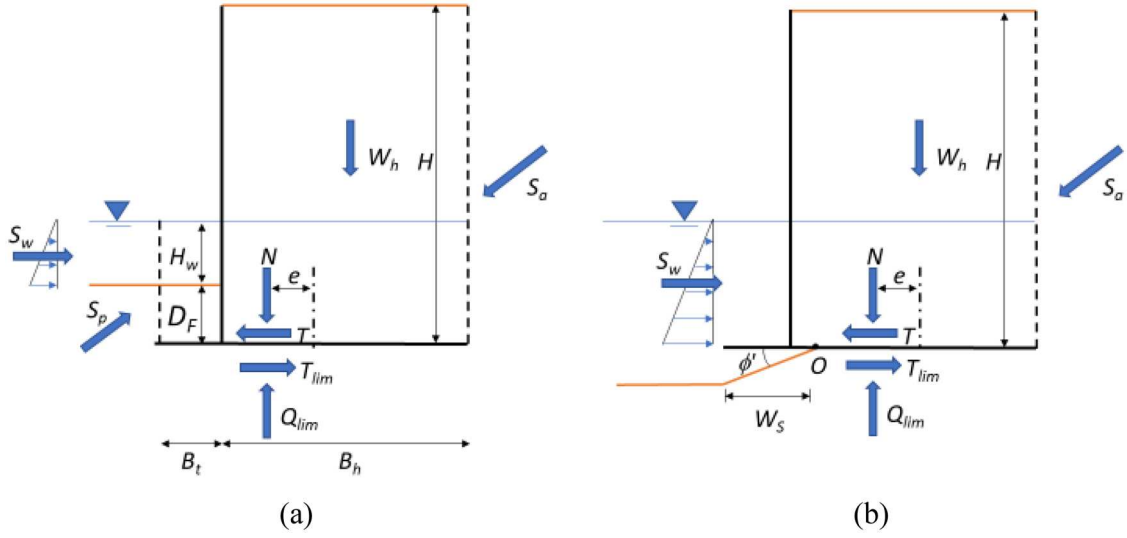

Figure 2. Sketch of a cantilever wall and relevant actions and resisting mechanisms for the case of (a) no scour, (b) scour undermining the foundation.

applied normal force N exceeds the limiting capacity $Q_{lim.}$ Sliding failure takes place when the driving shear force T surpasses the available resistance T_{lim}. Overturning failure happens when the destabilising moment exceeds the stabilising moment, with both these moments measured with respect to the point of intersection between the scour hole and the foundation base (i.e. point O in Figure 2(b)).

2.2. Active and passive thrusts

Accurate estimation of the active thrust S_a and passive thrust S_p is crucial for assessing the stability of retaining walls under all failure mechanisms. The earth pressures should also account for the impact of water. On the backfill side, water adds horizontal hydrostatic force to the active earth pressure on the lower portion of the wall. On the riverside, with water above the riverbed, the weight of water increases the passive pressure. The earth pressures are also affected by scour. With wall friction considered, scour changes the vertical component of passive pressure, therefore influencing sliding resistance, overturning moments and the overall geotechnical demand.

The active thrust S_a is given in Equations (3)–(5), and the passive thrust S_p is in Equations (6)–(8); their expressions are based on the coefficient k_a for active thrust and k_p for passive thrust derived using the lower bound theorem of plasticity (Lancellotta 2002). Each earth pressure consists of two parts, with a different pressure distribution and point of application, requiring separate consideration during moment equilibrium calculations for accurate stability assessment. $S_{ah,1}$ is the active pressure from the retained soil, whereas $S_{ah,2}$ accounts for hydrostatic water pressure, which acts partially on the lower portion of the soil-wall system. $S_{ph,1}$ is the passive pressure, and $S_{ph,2}$ represents the weight of overlying water, forming a rectangular pressure distribution. Both passive pressure components change with scour. Due to friction at the soil-wall interface, the effective vertical component of earth pressure forms an angle δ with the effective horizontal component, where δ is assumed equal to the soil friction angle ϕ'. It should be noted that the soil–wall interface is actually a soil–soil interface, since the soil above the heel is treated as an integral part of the retaining wall. The development of the expressions for earth pressures is illustrated in Appendix A.

$$S_{ah} = \underbrace{\frac{1}{2}k_a\gamma H^2}_{S_{ah.1}} + \underbrace{\frac{1}{2}(1-k_a)\gamma_w(H_w+D_F)^2}_{S_{ah.2}} \tag{3}$$

$$k_a = (1-\sin\phi')e^{-\left(\frac{\pi}{2}-\phi'\right)\tan\phi'} \tag{4}$$

$$S_{av} = \frac{1}{2}\tan\phi' k_a \gamma H^2 - \frac{1}{2}\tan\phi' k_a \gamma_w (H_w+D_F)^2 \tag{5}$$

$$S_{ph} = \underbrace{\frac{1}{2}\gamma k_p D_F'^2 + \frac{1}{2}(1-k_p)\gamma_w D_F'^2}_{S_{ph,1}} + \underbrace{\gamma_w(H_w+D_F-D_F')D'_F}_{S_{ph,2}} \tag{6}$$

$$k_p = (1+\sin\phi')e^{\left(\frac{\pi}{2}+\phi'\right)\tan\phi'} \tag{7}$$

$$S_{pv} = \frac{1}{2}(\gamma-\gamma_w)k_p^* = \tan\phi' k_p D_F'^2 \tag{8}$$

2.3. Bearing capacity

Scour impacts the bearing capacity by reducing the embedded depth and the effective soil-foundation interface, and this, in turn, changes the eccentricity and the inclination of the resultant load on the riverbed. The change in eccentricity further reduces the effective width of the foundation. To capture these effects, the bearing capacity formulation is developed for the three scenarios illustrated in Figure 1. The riverbed soil is assumed to be cohesionless and homogeneous, with its effective friction angle remaining unchanged by scour.

In the absence of scour, the effective bearing capacity q'_{lim} is given by the following expression based on Hansen and Vesić's approach (Hansen 1970; Vesić 1973):

$$q'_{lim} = \frac{1}{2}\gamma B' N_\gamma i_\gamma + \gamma D_F N_q i_q \tag{9}$$

where B' is the effective foundation width, given by

$$B' = B_h + B_t - 2e \tag{10}$$

In Equation (10), N_q and N_γ are dimensionless factors depending on the friction angle of the soil, and i_q and i_γ are surcharge inclination angles depending on the ratio between the horizontal and vertical force, T and N.

$$N_q = \frac{1+\sin\phi'}{1-\sin\phi'}\exp(\pi\tan\phi') \tag{11}$$

$$N_\gamma = 1.5(N_q-1)\tan\phi' \tag{12}$$

$$i_q = \left(1-\frac{T}{N}\right)^2 \tag{13}$$

$$i_\gamma = \left(1-\frac{T}{N}\right)^3 \tag{14}$$

For low scour depths such that the foundation is not undermined ($D_T \leq D_F$), q'_{lim} is given by

$$q'_{lim} = \frac{1}{2}\gamma B' N_\gamma i_\gamma + \gamma D F' N_q i_q \tag{15}$$

When scour reaches the base of the foundation ($D_T > D_F$), undermining a portion W_s of the foundation, q'_{lim} is given by

$$q'_{lim} = \frac{1}{2}\gamma B' N_\gamma i_\gamma \tag{16}$$

$$B' = (B_h + B_t - W_s) - 2e \tag{17}$$

A positive eccentricity e means the resultant force N is positioned to the left of the effective foundation centre. When scour occurs, but the foundation is not undermined (i.e. $D_T \leq D_F$), moment equilibrium results in an eccentricity with respect to the mid-point of the effective foundation by Equation (18).

$$e = \frac{W_t \frac{B_h}{2} + S_{ah,1}\frac{H}{3} + S_{ah,2}\frac{H_w + D_F}{3}}{W_t + W_h + S_{av} - S_{pv} - U} - \frac{W_h \frac{B_t}{2} + S_{av}\left(\frac{B_h + B_t}{2}\right) + S_{ph,1}\frac{D'_F}{3} + S_{ph,2}\frac{D'_F}{2} + S_{pv}\left(\frac{B_h + B_t}{2}\right) + S_w\left(\frac{H_w + D_T}{3} + D'_F\right)}{W_t + W_h + S_{av} - S_{pv} - U} \tag{18}$$

When scour undermines the foundation (i.e. $D_T > D_F$ and $Ws > 0$), moment equilibrium introduces eccentricity by Equation (19).

$$e = \frac{W_t \frac{B_h + W_s}{2} + S_{ah,1}\frac{H}{3} + S_{ah,2}\frac{H_w + D_F}{3} - W_h \frac{B_t - W_s}{2} - S_{av}\left(\frac{B_h + B_t - W_s}{2}\right)}{W_t + W_h + S_{av} - S_{pv} - U} + \frac{-S_w\left(\frac{H_w + D_F}{3}\right) - U\frac{W_s}{2}}{W_t + W_h + S_{av} - S_{pv} - U} \tag{19}$$

The total bearing force Q_{lim} is the sum of the effective bearing force and buoyancy force, given by

$$Q_{lim} = [q'_{lim} + \gamma_w(D_F + H_w)]B'L \tag{20}$$

2.4. Other actions and resisting mechanisms

The soil-foundation interface is subjected to resultant action forces, including a driving shear force T, which is the sum of horizontal earth pressures and horizontal water pressure, and a vertical resultant force N, which is the sum of the soil weight (adjusted for buoyancy) and vertical passive pressure. They are expressed as follows:

$$T = S_{ah} - S_{ph} - S_w \tag{21}$$

$$N = W_t + W_h + S_{av} - S_{pv} - U \tag{22}$$

The force applied to the toe W_t consists of the weight of the soil and of the water above it, influenced by scour actions. The force on the heel, $W_{h,}$ represents the weight of the retained soil and water, remaining unaffected by scour. These forces are expressed as follows:

$$W_t = B_t[D'_F\gamma + (H_w + D_F - D'_F)\gamma_w] \tag{23}$$

$$W_h = B_h\gamma H \tag{24}$$

where γ denotes the equivalent soil unit weight, which is the total weight of the saturated and unsaturated soil divided by the relevant overall soil volume.

The stem, i.e. the vertical structural element that directly retains the soil, is subject to the water thrust on the toe side, S_w, which increases as the soil layer diminishes and the scour progresses, whose expression is as follows:

$$S_w = \frac{1}{2}\gamma_w(H_w + D_F - D'_F)^2 \tag{25}$$

The wall-soil system is subject to the buoyancy force U, which is unaffected by scour and is given by

$$U = (H_w + D_F)(B_t + B_h)\gamma_w \tag{26}$$

3. Limit-state functions

Three different limit-state functions are formulated to describe the failure mechanisms, namely geotechnical failure, overturning failure and sliding failure. Geotechnical failure occurs if the vertical surcharge N exceeds the bearing capacity Q_{lim}, which corresponds to the bearing capacity factor f_{bc} defined below, exceeding 1:

$$f_{bc} = \frac{W_t + W_h + S_{av} - S_{pv}}{Q_{lim}} \tag{27}$$

Overturning failure occurs when the destabilising moments exceed the stabilising moments, i.e. when the overturning factor defined in Equation (28) exceeds 1. When the foundation is not undermined, overturning is measured at the edge of the foundation on the waterside. When scour undermines the foundation, the overturning of the retaining wall is measured at the point O of Figure 2(b). As scour progresses, this point moves past the centre of the toe, foundation and heel and stabilising forces are destabilising. To account for this, various expressions of the overturning factor need to be considered; these are detailed in Appendix B.

$$f_{ov} = \frac{M_{de}}{M_{st}} \tag{28}$$

where M_{st} and M_{un} denote the stabilising and destabilising moments, respectively.

Sliding failure occurs when the driving sliding force T exceeds the sliding resistance T_{lim}, which corresponds to the sliding factor f_{sl} defined below exceeding 1.

$$f_{sl} = \frac{S_{ah} - S_{ph} - S_w}{(W_t + W_h + S_{av} - S_{pv} - U)\tan\phi'} \tag{29}$$

4. Strength reduction method

The stability of retaining walls at any given scour D_T can be evaluated using the three failure mechanisms described above, each based on its respective limit state function. The factor of safety for each of these mechanisms is assessed via the Strength Reduction Method (SRM) (EN 1997). The partial safety factor $\gamma_{\phi'}$ represents the reduction factor of the shearing resistance required to bring the soil to the onset of collapse. The factor of safety is quantified as the ratio between the tangent of the actual friction angle, $\tan\phi'$, and the tangent of the friction angle associated with the onset of failure, $\tan\phi'_{crit}$.

$$\gamma_{\phi'} = \frac{\tan\phi'}{\tan\phi'_{crit}} \tag{30}$$

Let us consider the case of a retaining wall initially stable. To cause the retaining wall to fail, $\tan\phi'$ needs to be decreased to a critical value $\tan\phi'_{crit}$ until collapse occurs. The reduction in soil friction angle affects both the demand and capacity in all failure mechanisms; it increases the active thrust and reduces the passive thrust, respectively, thereby increasing the risk of sliding and overturning. At the same time, the lower friction angle underneath the foundation decreases the bearing capacity Q'_{lim} and decreases the sliding resistance T_{lim}, thus increasing the likelihood of failure by exceedance of bearing capacity and sliding.

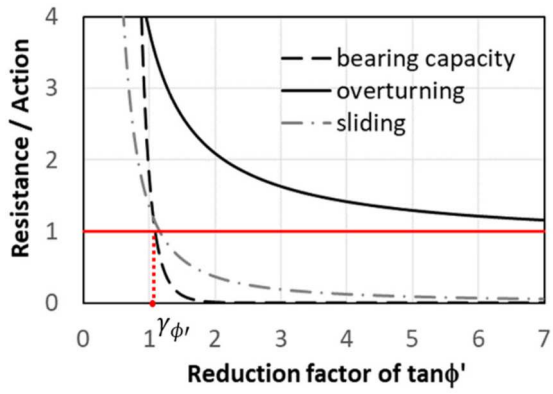

Figure 3. Resistance-to-action ratio and the reduction factor of $\tan\phi'$. Example of a retaining wall with the geometry of $H = 4.05$ m, $D_T = 0$, $B_h = 1.2$ m, $B_t = 1.3$ m, $D_F = H_w = \gamma_w = \delta = 0$, $\phi' = 28°$.

Figure 3 shows an example of the resistance-to-action ratio for the three failure mechanisms against the reduction factor. As the reduction factor increases, the soil friction angle reduces, and the resistance-to-action ratio also reduces. The intersection points between the resistance-to-action curve and the horizontal red line, where resistance-to-action equals 1, identify the partial safety factor for the individual mechanisms. The partial safety factor $\gamma_{\phi'}$ for the retaining wall is the minimum partial safety factor between the three mechanisms (the bearing capacity in the example shown in Figure 3). This corresponds to considering the system reliability as a series system, similarly to Daryani and Mohamad (2014).

5. Model validation

The proposed closed-form solution is validated against numerical modelling using three structures representative of retaining walls in the UK road transport network. For each case study, the curve describing the reduction in the safety factor with increasing scour levels, derived from sections 2–4, is compared with the corresponding curve obtained using PLAXIS (PLAXIS 2020).

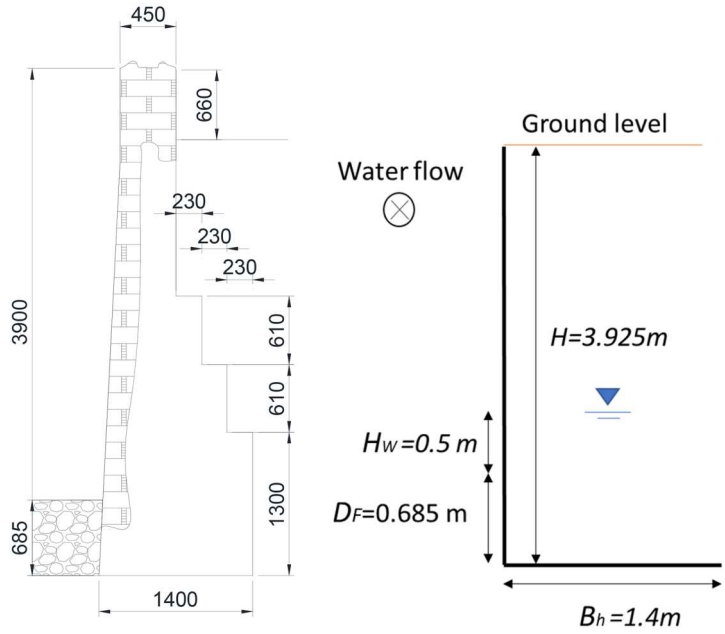

(a)

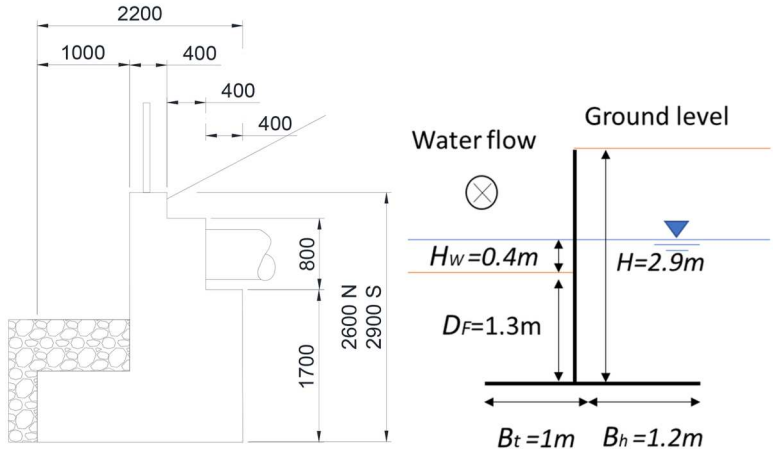

(b)

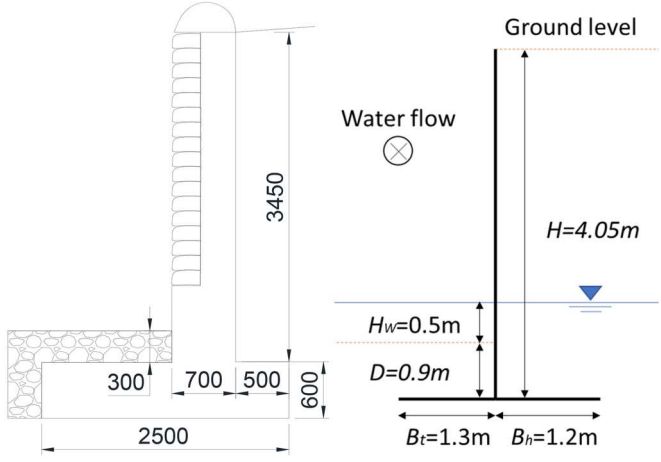

(c)

Figure 4. Section drawings of retaining walls adjacent to the riverbank and their equivalent geometry in the closed-form solution. (a) retaining wall 1 (RW1), (b) retaining wall 2 (RW2), (c) retaining wall 3 (RW3)

Figure 4 illustrates the transverse section of the walls and the corresponding simplified model used in the proposed formulation. The retaining wall in Figure 4(a) is modelled as a wall with no toe, whereas the one in Figure 4(b) is a wall with a toe and a heel. The retaining wall in Figure 4(c) is a typical cantilever wall with an inverted "T" shape, which mostly utilise the weight of the backfill soil to provide resistance to failure.

Numerical models of the selected case studies, developed in PLAXIS 3D Version 20.03 (PLAXIS 2020), are used to calculate the variation of the factor of safety with increasing scour levels. To eliminate the impact of the boundaries on the results, the soil domain's height and width are set to be 8 times and 10 times the height of the wall, respectively. The ground has the displacement constrained in the out-of-plane direction to simulate a plane strain state. The mesh is refined into three zones, becoming progressively finer near the wall to enhance the accuracy of capturing soil deformation in its vicinity. The backfill and foundation soil are modelled with a homogeneous elasto-plastic material model with the failure surface described by the Mohr–Coulomb criterion, defined by the parameters Young's modulus E'_{ref} (kN/m^2), Poisson's ratio ν, friction angle ϕ'(°), Dilatancy angle ψ' (°), Cohesion c' (kPa). It is noteworthy that the value of the friction angle of 20° used for the analysis of RW2 is rather low and has been considered here purely as an illustrative example, representing loose alluvial soils from riverbed material with low strength and bearing capacity. The retaining wall is represented by an elastic material with Young's modulus representing concrete with a compressive strength of 25 MPa (ACI 2011). Between the soil and the wall, interface elements are introduced. The stiffness and strength properties of the interfaces are derived from those of the surrounding soil. Table 1 illustrates the values adopted for the parameters of the three models.

Each case study was analysed in PLAXIS using a three-stage construction procedure. In the first stage, the retaining wall and the initial ground conditions were activated and brought to equilibrium. In the

Table 1. Values of parameters of PLAXIS models.

Soil properties						Wall Properties		
Young's modulus E'_{ref}(kN/m^2)	Poisson's ratio ν	Friction angle ϕ' (°)	Dilatancy angle ψ' (°)	Cohesion c' (kPa)	Bulk density γ(kN/m^3)	Young's modulus E'_{ref} (kN/m^2)	Poisson's ratio ν	Density (kN/m^3)
25700	0.286	RW1: 35 RW2: 20 RW3: 28	RW1: 35 RW2: 20 RW3: 28	0	20	23500000	0.15	25

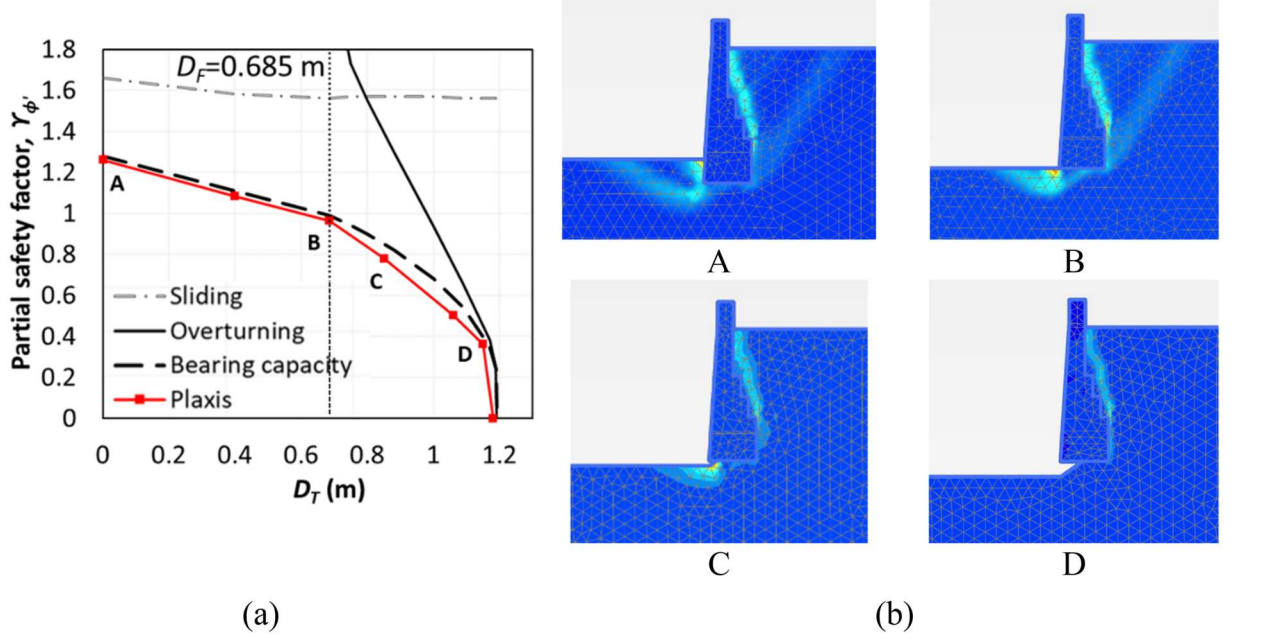

Figure 5. Partial safety factor under scour for RW1 (a) closed-form solution and PLAXIS, (b) incremental deviatoric strains contours show failure planes.

second stage, the scour process was simulated by progressively removing soil elements around the wall until a new equilibrium state was achieved. In the final stage, a strength-reduction analysis was performed, in which the shear strength parameters ϕ' and c were systematically reduced to identify the onset of global failure of the retaining wall system.

Figures 5–7 illustrate the contour plot of the incremental deviatoric strains ε_q at the final step of the analysis for the selected case studies, under conditions of no scour and varying scour levels. The patterns of incremental deviatoric strains are similar at point A (no scour) and point B (scour depth equal to embedment depth). In both situations, failure planes develop across the backfill soil and extend below the foundation and towards the riverbed. When the foundation is undermined by scour (point C), the failure surfaces are still located below the foundation and within the backfill soil, but the affected area is smaller than in previous stages, suggesting a localisation of deformations. As scour progresses further (point D), the deviatoric strains are concentrated primarily near the back of the wall, suggesting that the overturning mode becomes critical when the critical scour condition is approached.

Figures 5–7 also show the curves describing the reduction of safety factor based on the closed-form solutions for sliding, overturning and foundation bearing capacity limit state, and the curve derived from the

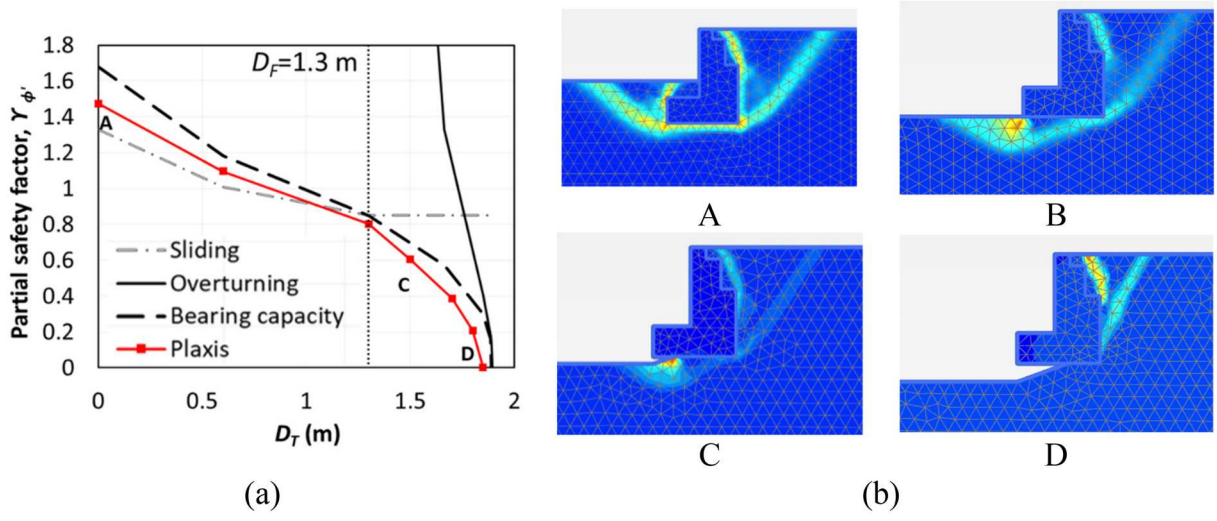

Figure 6. Partial safety factor under scour for RW2 (a) closed-form solution and PLAXIS, (b) incremental deviatoric strains contours show failure planes.

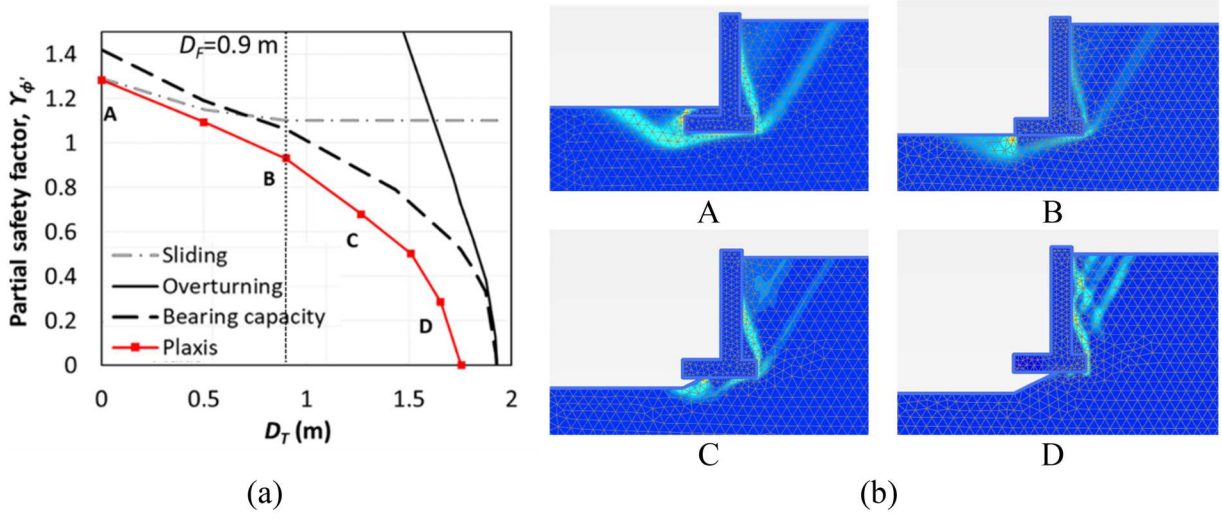

Figure 7. Partial safety factor under scour for RW3 (a) closed-form solution and PLAXIS, (b) incremental deviatoric strains contours show failure planes.

numerical analysis. For $D_T < D_F$, the sliding failure is the critical failure mechanism in RW2 and RW3. However, as scour progresses ($D_T \geq D_F$), the foundation bearing capacity limit state is characterised by the lowest safety factor and controls the failure. It is also worth observing that the curves for the overturning and bearing capacity limit state tend to converge to the same point at zero capacity. According to the proposed formulation, this point corresponds to the location of the resultant of the vertical loads. If the horizontal penetration of scour progresses beyond this point, equilibrium is not possible. This observation has important implications for the definition of a simplified expression for the reduction of the safety of retaining walls due to scour in Sections 2–4.

In general, it is interesting to observe that for low levels of scour, the safety factor reduces almost linearly for increasing scour levels, whereas for high levels of scour, a nonlinear, more significant reduction is observed until the critical condition of zero capacity is attained. Despite its underlying simplifying assumptions, the proposed formulation provides results quite close to the numerical results. The discrepancy between the results can be attributed mainly to the assumption of independent failure mechanisms and the fact that the bearing capacity is calculated using a semi-empirical approach to account for the eccentricity of the vertical force.

6. Non-dimensional formulation

The partial safety factor for retaining walls subjected to scour is affected by several geometrical and mechanical parameters, including the wall height H, width of base B, width of toe B_t, embedded depth D_F, water depth H_w-$+D_F$, friction angle of the base soil and retained soil ϕ', unit weight of the base soil and retained soil γ. In order to reduce the number of independent variables and highlight the most influential ones that control the problem, a dimensional analysis, using Buckingham's Pi theorem (Buckingham 1914), is carried out. This approach is useful in parametric studies investigating various scenarios, by also preserving the relationships between parameters in a manner consistent with practical design principles. For instance, in the design of cantilever walls, the height-to-base width ratio typically falls within the range of 1 to 2. Table 2 illustrates the identified non-dimensional parameters and their range of variation, representing typical retaining wall designs in engineering practice (Kaveh, Biabani Hamedani, and Zaerreza 2021; Sarıbaş and Erbatur 1996 Uray et al. 2020;). Table 2 illustrates the identified non-dimensional parameters and their range of variation, representing typical retaining wall designs in engineering practice (Kaveh, Biabani Hamedani, and Zaerreza 2021; Sarıbaş and Erbatur 1996 Uray et al. 2020;). Regarding the water level, $(H_w+D_F)/H$ is assumed to vary between 0 and 0.6, where H_w+D_F represents the portion of the retaining wall below the water level. Accordingly, the relative footing depth D_F/H is assumed to fall within the range 0–0.3, and the normalised water depth H_w/H is likewise taken to vary between 0 and 0.3. It should be noted that higher relative water levels than those investigated may occur during extreme events, leading to scour. However, considering a wider range of variation for H_w has no impact on the observed results.

Table 2. Non-dimensional parameters controlling the problem and range of values.

Non-dimensional parameters				
	Influencing parameters	Symbol	Lower bound	Upper bound
Π1	Embedded depth of the wall// Height of the wall	D_F/H	0	0.3
Π2	Width of the toe/width of the wall base	B_t/B	0	0.5
Π3	Height of the wall /width of the wall base	H/B	1	2
Π4	Friction angle of the base soil and retained soil	ϕ'	0.38	0.7
Π5	Unit weight of the soil /Unit weight of water	γ/γ_w	1.6	2.8
Π6	Water level to foundation base level/Height of the wall	H_w/H	0	0.3
Π7	Normalised scour demand	D_T/D_{Tlim}	0	1
Influenced variable				
	Partial factor under scour /partial factor at zero scour	$\gamma_{\phi'}/\gamma_{\phi'_0}$	0	1

To account for retaining walls characterised by a frictional behaviour at the wall-soil interface ($\delta > 0$), the interface friction angle is assumed equal to the soil's internal friction angle ($\delta = \phi'$). Moreover, to define the scour demand, the limit value of the scour depth is introduced, D_{Tlim}, defined as follows:

$$D_{Tlim} = D_F + (B_t + B_h/2) \cdot tan\phi' \tag{31}$$

The value of D_{Tlim} represents the condition where the foundation is undermined up to the centre of the heel. At this stage, the remaining soil beneath the heel cannot resist vertical gravitational forces corresponding to the retained soil, and thus stability is not possible regardless of the value of ϕ', i.e., $\frac{\gamma_{\phi'}}{\gamma_{\phi'_0}} = 0$. The results obtained for the previously analysed case studies confirm this. The value of D_{Tlim} for RW1, RW2 and RW3 is 1.9, 1.9, and 1.2 m respectively, which corresponds to the points where $\gamma_{\phi'} = 0$ in Figure 5(a), Figure 6(a) and Figure 7(a). As will be shown below, the proposed non-dimensional scour measure enables the identification of a

single master curve, providing a unified, scaled representation onto which all data points, regardless of material or conditions.

In order to evaluate the influence of the non-dimensional parameters on the safety of retaining walls for different levels of scour, $N_{samples} = 6380$ combinations of the non-dimensional parameters are generated, assuming uniform distributions between their respective lower and upper bounds. For each sample combination, corresponding to a wall-soil-water configuration, the normalised partial safety factor $\frac{\gamma_{\phi'}}{\gamma_{\phi'_0}}$ is determined for increasing values of the dimensionless scour depth $\frac{D_T}{D_{Tlim}}$ in the range from 0 to 1. The relationship between $\frac{\gamma_{\phi'}}{\gamma_{\phi'_0}}$ and $\frac{D_T}{D_{Tlim}}$ is then plotted, considering the combined effects of the multiple variables. Figure 8 illustrates the result of the analysis for the case of $D_F/H = 0$ and $D_F/H \geq 0$. Despite significant variations in wall geometry, water depth and soil properties, the reduction in the safety factor collapses onto a single master curve (red curve in Figure 8(a)). Notably, in the case of $D_F/H = 0$ (a), the data exhibit minimal scatter from the master curve, which means that the reduction of the normalised partial factor is governed solely by the normalised scour depth and is independent of other non-dimensional parameters. The master curve can be approximated by Equation (32):

$$\frac{\gamma_{\phi'}}{\gamma_{\phi'_0}} = \left(1 - \frac{D_T}{D_{Tlim}}\right)^{0.4} \tag{32}$$

When $D_F/H \geq 0$ (Figure 8(b)), the variance of the data points and the scatter from the master curve increase. To investigate the source of variance under different levels of scour, global sensitivity analysis (Sobol 2001) is carried out to quantify the contribution of each variable and their interaction to the variance of the model output $\frac{\gamma_{\phi'}}{\gamma_{\phi'_0}}$. The sensitivity analysis is carried out at fixed values of the normalised scour depth, corresponding to values of $\frac{D_T}{D_{Tlim}}$ of 0.15, 0.3, 0.45, 0.6, 0.75 and 0.9. At each scour level, the total output variance $V\left(\frac{\gamma_{\phi'}}{\gamma_{\phi'_0}}\right)$ is evaluated by the variance of the expected value of $\frac{\gamma_{\phi'}}{\gamma_{\phi'_0}}$ conditioned on a fixed value of Π_i. The second-order effect, V_{ij}, is the joint effect of Π_i and Π_j minus the first-order effects for the same factor. The contribution of each input to the output variability is represented by the Sobol indices. The first-order Sobol index S_i quantifies the effect of input Π_i, while the total Sobol index S_{T_i} includes first-order effects of input Π_i plus all higher-order effects due to interaction.

The sensitivity analysis is conducted using the SobolGSA toolbox (Kucherenko 2013). The nondimensional factors are treated as independent random variables with uniform distributions over their respective ranges.

Figure 9 presents the sensitivity indices of $\Pi_1, \Pi_2, \ldots, \Pi_6$ under different levels of scour. In general, it can be observed that these indices vary significantly with scour. In the early scour stage

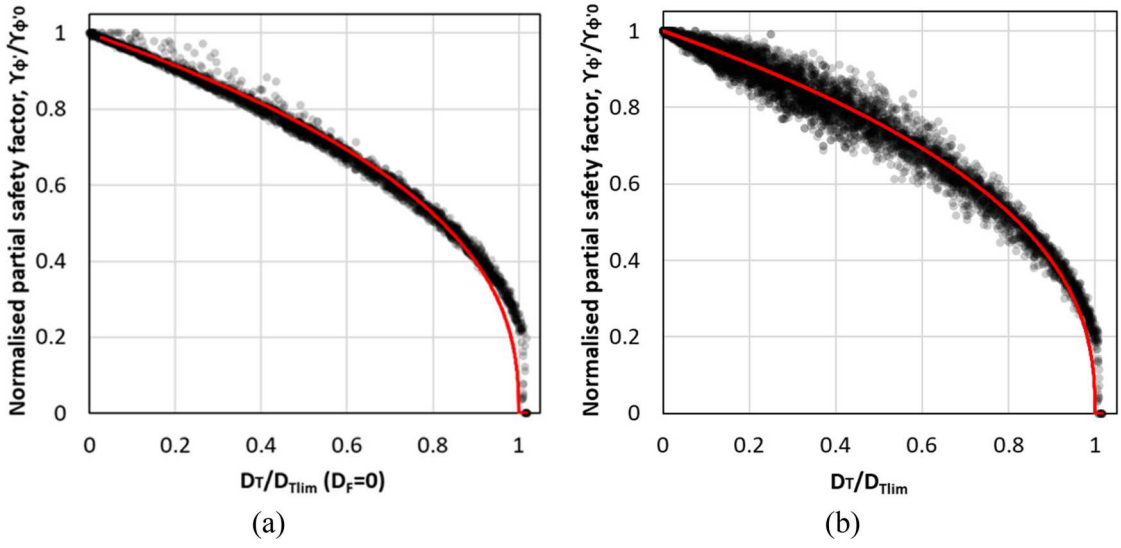

Figure 8. The reduction of the partial safety factor under progressive scour $\frac{D_T}{D_{Tlim}}$ for (a) $D_F/H = 0$, (b) $D_F/H \geq 0$.

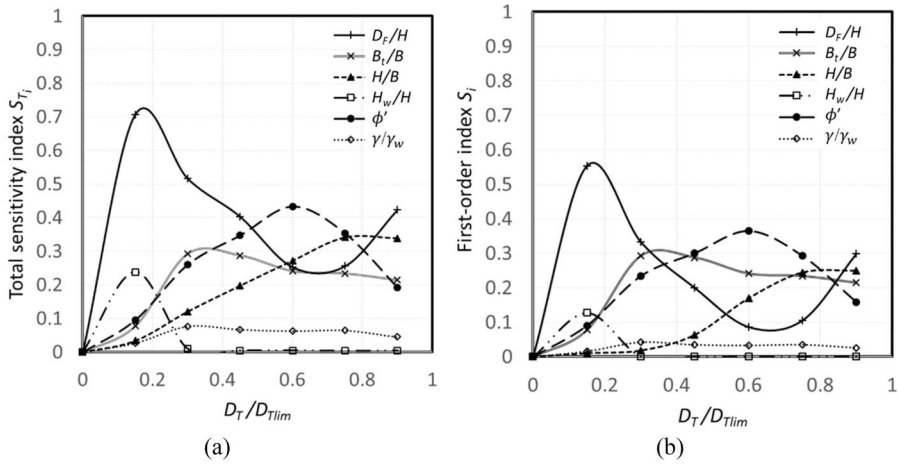

Figure 9. Sensitivity indices of non-dimensional variables under fix value of scour: (a) total sensitivity indices, (b) first-order indices.

($\frac{D_T}{D_{Tlim}} < 0.15$), D_F/H and H_w/H govern the output uncertainty, then their contribution gradually reduces. The total index for D_F/H stays above 0.2, while that for H_w/H drops to a negligible value after $\frac{D_T}{D_{Tlim}} = 0.3$. In contrast, the indices for B_t/B, H/B and ϕ' increase with scour and play secondary roles. The total sensitivity index of B_t/B rises from 0 to 0.3, then remains nearly flat with a slight decline to a value of 0.2. Meanwhile, the total sensitivity index of H/B consistently increases from 0 to 0.35 until $\frac{D_T}{D_{Tlim}} = 0.75$. The increasing impact of H/B suggests the involvement of overturning failure, as higher H/B increases active pressure and the risk of overturning under the same scour conditions. The total sensitivity index of ϕ' increases from zero at the unscoured condition, peaks at 0.45, then decreases to 0.2, showing a hump trend. This reflects that ϕ' has double effects on the stability of retaining walls; a higher value of ϕ' increases the stability of the wall-soil system, but it can make it more unstable by steepening the inclination of the scour hole under the wall base. Compared with other variables, γ/γ_w has a negligible impact on the results and remains flat throughout.

The main outcome of the global sensitivity analysis is that many non-dimensional parameters have an impact on the output variance, and this impact changes with the scour depth. Thus, it is unpractical to attempt to derive an expression more sophisticated than Equation (32) to explicitly describe the effect of each parameter on the reduction of the safety factor. Rather than doing this, it is preferable to keep Equation (32) to estimate $\frac{\gamma_{\phi'}}{\gamma_{\phi'_0}}$ and derive a simple expression for quantifying its uncertainty. For this purpose, the relative squared errors (ε_i^2, $i = 1, 2,.., N_{samples}$) and coefficient of variation (cov_s) are evaluated for increasing values of the normalised scour. We remind the reader that the relative squared error ε_i^2 of the i-th sample is defined as the square of the difference between the fitted values implied by Equation (32) and the true value from the closed-form solution, divided by the true value. Figure 10 plots the relative squared errors ε_i^2 of the samples as a function of $\frac{D_T}{D_{Tlim}}$ and an estimate of cov_s^2 obtained using a moving average method. It can be observed that the uncertainty cov_s^2 is zero when the scour is zero, increases progressively with scour until $\frac{D_T}{D_{Tlim}} = 0.5$,

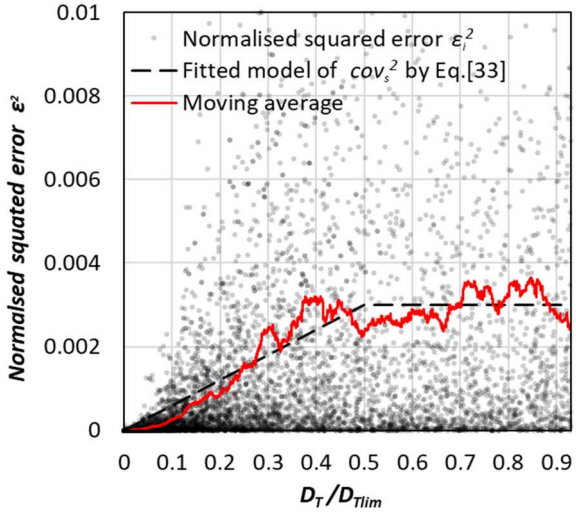

Figure 10. Variation of normalised squared error ε^2 and cov_s^2 with increasing scour.

after which it is effectively constant. Based on this observation, a simplified expression can be derived for cov_s^2:

$$\mathrm{cov}_s^2 = min\left(0.06\frac{D_T}{D_{Tlim}}, 0.003\right) \tag{33}$$

7. Scour vulnerability model

In this section, a simplified model is derived for the scour vulnerability of retaining walls, based on reliability-based principles. This model links the probability of a failure condition to the scour level by exploiting the closed-form expressions derived in the previous section for the mean reduction of the normalised safety factor due to scour and its coefficient of variation.

The safety factor $\gamma_{\phi'}$ of the retaining wall associated with the most critical failure mode is an uncertain quantity, whose variability depends on the design uncertainties and the additional uncertainty in capacity brought by scour. Assuming that $\gamma_{\phi'}$ is a random variable with lognormal distribution, mean value $E(\gamma_{\phi'})$ and coefficient of variation cov_Z, the probability of failure of the retaining wall can be expressed as follows:

$$P_F = \Phi(-\beta) \tag{34}$$

where Φ is the cumulative standard normal distribution and β is Rosenblueth's and Esteva's reliability index (Rosenblueth and Esteva 1972), expressed by

$$\beta = \frac{\ln E(\gamma_{\phi'})}{cov_Z} \tag{35}$$

The uncertainty of the safety factor cov_Z combines the design uncertainty cov_0 and the additional uncertainty introduced by scour cov_s according to

$$cov_Z = \sqrt{cov_0^2 + cov_s^2} \tag{36}$$

where uncertainty cov_s is quantified by equation (33), and the design uncertainty cov_0 is evaluated by a retaining wall with no scour. Similar to the general case, the reliability index β_0 depends on the mean value of the design safety factor $E(\gamma_{\phi'_0})$ and the design uncertainty cov_0 through Rosenblueth's and Esteva's formula:

$$\beta_0 = \frac{E(\gamma_{\phi'_0})}{cov_0} \tag{37}$$

The design reliability β_0 depends on the level of overdesign of the retaining wall. It should be noted that the target failure probabilities of retaining walls are still very much unknown (He, Fenton, and Griffiths 2022). According to Eurocode guidelines, a target reliability index β_0 of 3.8 is considered acceptable for designing retaining wall-type structures under ultimate limit states (EN 1990:2002), and a nominal partial factor $\gamma_{\phi'_0}$ of 1.25 is recommended for the soil friction angle to have adequate safety margins in design under ultimate limit states (EN 1997). Assuming that the retaining walls were properly designed in compliance with the Eurocode requirements, with no overdesign, the design coefficient of variation cov_0 can be estimated as follows:

$$cov_0 = \frac{\ln \gamma_{\phi'_0}}{\beta_0} = \frac{\ln 1.25}{3.8} \approx 6\% \tag{38}$$

Regarding the design situation, scour reduces the reliability of the retaining wall as it reduces the wall's mean safety factor (as per equation (32)) and increases its uncertainty (as per equation (33)). It is convenient to rearrange equation (37) to highlight the contribution of the design reliability β_0. In formula:

$$\begin{aligned}\beta &= \frac{\ln E(\gamma_{\phi'})}{cov_Z} = \frac{\dfrac{\ln E(\gamma_{\phi'_0})}{cov_0} cov_0 + \ln \dfrac{E(\gamma_{\phi'})}{E(\gamma_{\phi'_0})}}{cov_Z} \\ &= \frac{\beta_0 \cdot cov_0 + \ln E\left(\dfrac{\gamma_{\phi'}}{\gamma_{\phi'_0}}\right)}{\sqrt{cov_0^2 + cov_s^2}}\end{aligned} \tag{39}$$

where we have accepted the approximation:

$$\frac{E(\gamma_{\phi'})}{E(\gamma_{\phi'_0})} \cong E\left(\frac{\gamma_{\phi'}}{\gamma_{\phi'_0}}\right) \tag{40}$$

The loss in reliability $\Delta\beta$ caused by scour can also be expressed in closed form by

$$\begin{aligned}\Delta\beta &= \beta - \beta_0 \\ &= \beta_0\left(\frac{cov_0}{\sqrt{cov_0^2 + cov_s^2}} - 1\right) + \frac{\ln E\left(\dfrac{\gamma_{\phi'}}{\gamma_{\phi'_0}}\right)}{\sqrt{cov_0^2 + cov_s^2}}\end{aligned} \tag{41}$$

Equation (39), together with (34), effectively provides an expression for the retaining wall's vulnerability as a function of the normalised scour depth $\frac{D_T}{D_{Tlim}}$:

$$P_F = \Phi(-\beta) = \Phi\left(-\frac{\beta_0 \cdot cov_0 + \ln E\left(\dfrac{\gamma_{\phi'}}{\gamma_{\phi'_0}}\right)}{\sqrt{cov_0^2 + cov_s^2}}\right) \tag{42}$$

Equation (42) indicates that the scour vulnerability of retaining walls depends on four factors:

- the design reliability β_0 generally provided by (37) or conservatively assumed to be equal to 3.8;
- the design uncertainty cov_0 , which can be assumed equal to 6% as per (38);
- the expected loss in safety factor $E\left(\frac{\gamma_{\phi'}}{\gamma_{\phi'_0}}\right)$ due to scour, quantified by (32);
- the additional uncertainty cov_s introduced by scour, quantified by (33)

To illustrate the simplicity and practical effectiveness of the method, the vulnerability curves are derived for the three retaining walls with varying geometries shown in Figure 4. Table 3 lists the values of the wall and soil parameters needed to estimate D_{Tlim} which include the toe width, heel width and embedded depth, extracted from the section drawing of the retaining walls, as well as the soil friction angle representative of the riverbed material, which is assumed. The value of β_0 can be assumed equal to 3.8 without performing any analysis of the retaining wall, based on the assumption that the wall satisfies the minimum reliability requirements. Alternatively, a more accurate β_0 value can be estimated by the nominal partial safety factor $\gamma_{\phi'_0}$ in the case of no scour, which is evaluated by using the proposed closed-form method, together with cov_0 in Equation (38).

Table 3. Input parameters for estimating the probability of failure of retaining walls under scour.

Case studies	Embedded depth D_F (m)	Soil friction angle ϕ' (°)	Toe width B_t (m)	Heel width B_h (m)	$\gamma_{\phi'_0}$	β_0
RW1	0.685	35	0	1.4	1.28	3.9
RW2	1.3	20	1	1.3	1.33	4.8
RW3	0.9	28	1.3	1.2	1.29	4.2

Figure 11 shows the vulnerability curves obtained for the selected case studies, conditional to the level of scour, as described by D_T or $\frac{D_T}{D_{Tlim}}$, in both the linear and semi-logarithmic scales. The curves in Figure 11(a) have been derived considering the values of β_0 reported in Table 3, corresponding to the actual values of $\gamma_{\phi'_0}$. The baseline vulnerability curve obtained for the Eurocode's target reliability $\beta_0 = 3.8$ is also plotted in the same figures, as dashed curves, for comparison. As expected, the probability of failure increases with

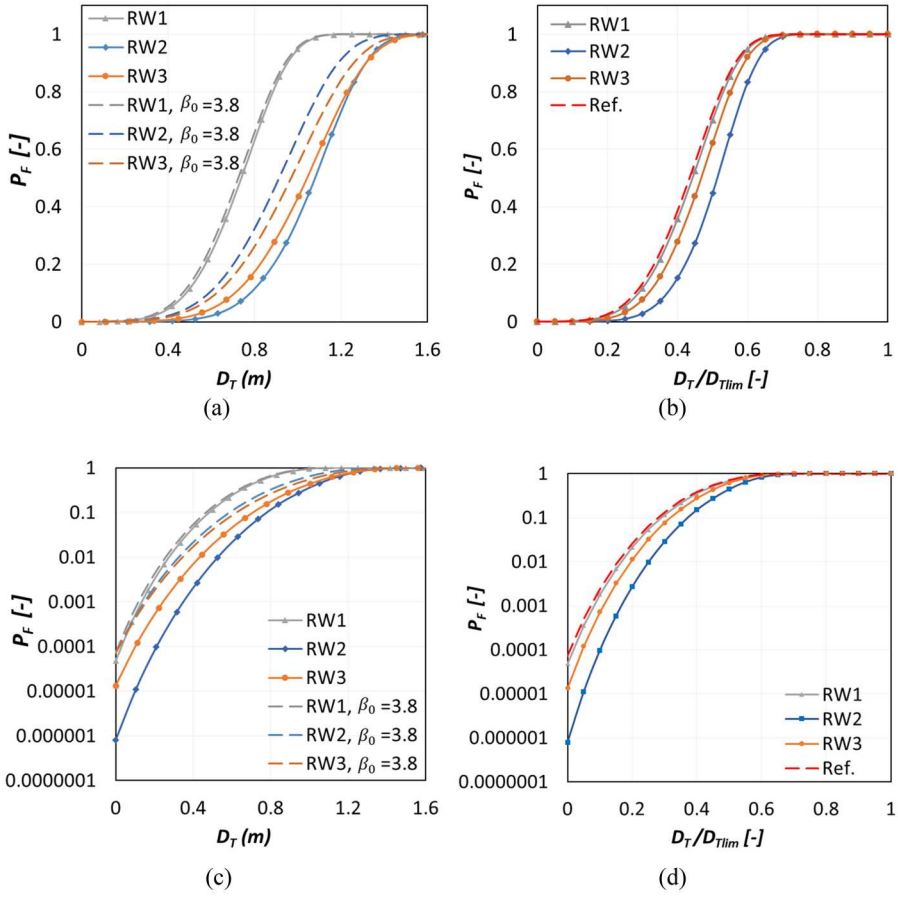

Figure 11. Vulnerability curves of the retaining walls (a) dimensional scour presentation, (b) non-dimensional scour presentation, (c) dimensional scour on a logarithmic scale of P_F, (d) non-dimensional scour on a logarithmic scale of P_F.

scour and differs for the various walls. When the scour depth is expressed in a dimensionless form, the vulnerability curves are closer to each other, and they differ only due to their different design reliability β_0, i.e. due to their different overdesign. Therefore, the baseline vulnerability curves, which have the same $\beta_0 = 3.8$, coincide in Figure 11(b) and are represented by the red dashed curve (i.e. the Ref. curve).

The vulnerability curves on a logarithmic scale highlight the impact of scour on the probability of failure across several orders of magnitude (Figure 11(c) and (d)). At zero scour depth, each retaining wall starts from a different value of probability of failure, with RW2 having the lowest value ($1e^{-6}$) and the reference case with the highest value ($7.5e^{-5}$). The failure probability rises sharply by several orders of magnitude due to scour: in the reference case, the failure probability increases by one, two and three orders of magnitude for values of the normalised scour level of 0.07, 0.15 and 0.28. It is also worth observing that the failure probability reaches the value of 1 when $\frac{D_T}{D_{Tlim}}$ approaches 0.7, regardless of the initial value of β_0. Use of the reference curve is recommended in the absence of more detailed information on the overdesign level, since it provides conservative estimates of the vulnerability.

8. Conclusion

This study has introduced a novel, simplified analytical approach to evaluate the safety of retaining walls under scour conditions, effectively addressing a key gap in the assessment of their vulnerability. The analytical approach commonly used for the stability analysis of retaining walls has been extended in this study to account for the effects of scour on the most critical failure mechanisms – namely, overturning, sliding and loss of base support. Closed-form expressions have been developed and validated against numerical modelling using three representative retaining walls in the UK transport network, showing good accuracy across a range of wall geometries, soil properties and hydraulic conditions. Moreover, by expressing the problem in dimensionless terms and applying global sensitivity analysis, the study has proposed a nondimensional scour measure, which enables the identification of a single master curve that provides a unified and scaled representation of the safety factor reduction, regardless of the variation in wall configurations, water depths and riverbed and soil properties. Finally, a model for the scour vulnerability of retaining walls has been developed based on a reliability-based framework, by exploiting the closed-form expressions for the mean safety factor reduction and its coefficient of variation.

The proposed method enables rapid estimation of scour vulnerability of retaining walls using basic input parameters, making it suitable for infrastructure asset management and prioritising maintenance and intervention strategies in flood-prone areas. Future work will extend this method to other retaining wall typologies (e.g. gabion walls, diaphragm walls and anchored walls) and will also provide practical guidelines for implementation in scour risk assessment and management procedures.

Author contributions

CRediT: **Lanting Wei:** Data curation, Formal analysis, Investigation, Methodology, Software, Validation, Visualization, Writing – original draft, Writing – review & editing; **Alessandro Tarantino:** Conceptualization, Data curation, Formal analysis, Investigation, Methodology, Software, Supervision, Validation, Visualization, Writing – original draft, Writing – review & editing; **Enrico Tubaldi:** Conceptualization, Data curation, Formal analysis, Funding acquisition, Investigation, Methodology, Project administration, Software, Supervision, Validation, Visualization, Writing – original draft, Writing – review & editing; **Hamed Moghaddasi:** Supervision, Validation; **Daniele Zonta:** Conceptualization, Formal analysis, Investigation, Methodology, Supervision, Writing – review & editing.

Disclosure statement

No potential conflict of interest was reported by the author(s).

Funding

The authors gratefully acknowledge the support of the Engineering and Physical Sciences Research Council (EPSRC) through the Innovation Launchpad Network+ Researcher in Residence scheme (Grant Nos. EP/W037009/1 and EP/X528493/1), in collaboration with Connected Places Catapult. Additional support was provided by National Highways through the project "Foundations: Improving Risk Assessment and Prioritisation Processes for the Management of Scour at Structures."

References

ACI. 2011. Building Code Requirements for Structural Concrete (ACI 318-11), American Concrete Institute.

Argyroudis, S. A., and S. A. Mitoulis. 2021. "Vulnerability of Bridges to Individual and Multiple Hazards- Floods and Earthquakes." *Reliability Engineering & System Safety* 210:107564. https://doi.org/10.1016/j.ress.2021.107564

Buckingham, E. 1914. "On Physically Similar Systems; Illustrations of the use of Dimensional Equations." *Physical Review* 4 (4): 345–376. https://doi.org/10.1103/PhysRev.4.345

Cely Calixto, N. J., A. Galvis Castaño, and G. A. Carrillo Soto. 2023. "Evaluation of Local Scour along the Base of Longitudinal Training Walls." *Water* 15 (22): 4001. https://doi.org/10.3390/w15224001

Cerema. 2019. Analyse de risque des ponts en site affouillable (in French). Collection: Références.

Daryani, K. E., and H. Mohamad. 2014. "System Reliability-Based Analysis of Cantilever Retaining Walls Embedded in Granular Soils." *Georisk: Assessment and Management of Risk for Engineered Systems and Geohazards* 8 (3): 192–201. https://doi.org/10.1080/17499518.2014.937583.

EN. 1997. Eurocode 7 Geotechnical Design—Part 1: General Rules.

EN (1990:2002). Eurocode: Basis of Structural Design.

Fael, C. S., G. Simarro-Grande, J. P. Martín-Vide, and A. H. Cardoso. 2006. "Local Scour at Vertical-wall Abutments under Clear-Water Flow Conditions." *Water Resources Research* 42:1–12. https://doi.org/10.1029/2005WR004443.

Hansen, J. B. 1970. "A Revised and Extended Formula for Bearing Capacity.".

He, P., G. A. Fenton, and D. V. Griffiths. 2023. "Calibration of Resistance Factors for Gravity Retaining Walls." *Georisk: Assessment and Management of Risk for Engineered Systems and Geohazards* 17 (3): 586–594.

Heydari, N., and P. Diplas. 2020. "Flow Dynamics in the Vicinity of a Gravel Embedded Vertical Retaining Wall: Conditions Corresponding to the Initial Stages of Local Erosion." *Environmental Fluid Mechanics* 20 (1): 203–225. https://doi.org/10.1007/s10652-019-09715-8.

Huang, C.-C. 2017. "Failure Mechanisms of Steep-faced Geosynthetic-Reinforced Retaining Walls Subjected to toe Scouring." *Marine Georesources & Geotechnology* 35 (8): 1099–1110. https://doi.org/10.1080/1064119X.2017.1290170.

Kaveh, A., K. Biabani Hamedani, and A. Zaerreza. 2021. "A Set Theoretical Shuffled Shepherd Optimization Algorithm for Optimal Design of Cantilever Retaining Wall Structures." *Engineering with Computers* 37 (4): 3265–3282. https://doi.org/10.1007/s00366-020-00999-9.

Khosronejad, A., P. Diplas, D. Angelidis, Z. Zhang, N. Heydari, and F. Sotiropoulos. 2020. "Scour Depth Prediction at the Base of Longitudinal Walls: A Combined Experimental, Numerical, and Field Study." *Environmental Fluid Mechanics* 20 (2): 459–478. https://doi.org/10.1007/s10652-019-09704-x.

Kirby, A. M., M. Roca, A. Kitchen, M. Escarameia, and O. J. Chesterton. April 2015. Manual on Scour at Bridges and Other Hydraulic Structures. 2nd ed. CIRA: London.

Kitchen, A., M. Roca, A. M. Kirby, and M. Escarameia. May 2021. Manual on Scour at Bridges and Other Hydraulic Structures - Supplementary Guide (SP171). CIRIA: London.

Kucherenko, S. 2013. "SobolHDMR: A General-purpose Modeling Software." *Methods in Molecular Biology* 1073:191–224. https://doi.org/10.1007/978-1-62703-625-2_16.

Lancellotta, R. 2002. "Analytical Solution of Passive Earth Pressure." *Géotechnique* 52 (8): 617–619. https://doi.org/10.1680/geot.2002.52.8.617.

McKelvey, J. A. I. I. I. 2011. "Lessons Learned from Failures: The Wall of Shame." In Geo-Frontiers 2011: Advances in Geotechnical Engineering, 3235–3244.

NationalHighways. 2024. CS 469 - Management of Scour and Other Hydraulic Actions at Highway Structures.

PLAXIS. 2020. PLAXIS 3D Reference Manual CONNECTION edition V20.03.

Rosenblueth, E., and L. Esteva. 1972. Reliability Basis for Some Mexican Codes.

Sarıbaş, A., and F. Erbatur. 1996. "Optimization and Sensitivity of Retaining Structures." *Journal of Geotechnical Engineering* 122 (8): 649–656. https://doi.org/10.1061/(ASCE)0733-9410(1996)122:8(649).

Scozzese, F., E. Tubaldi, and A. Dall'Asta. 2023. "Damage Metrics for Masonry Bridges under Scour Scenarios." *Engineering Structures* 296:116914. https://doi.org/10.1016/j.engstruct.2023.116914.

Sobol, I. M. 2001. "Global Sensitivity Indices for Nonlinear Mathematical Models and their Monte Carlo Estimates." *Mathematics and Computers in Simulation* 55 (1): 271–280. https://doi.org/10.1016/S0378-4754(00)00270-6.

Sotiropoulos, F., and P. Diplas. 2017. "Scour at the Base of Retaining Walls and Other Longitudinal Structures: Final Report." NCHRP, Transportation Research Board, The National Academies.

Theinat, A. K., R. Salgado, M. Prezzi, and V. A. Sakleshpur. 2024 . "Stability and Factor of Safety of Gravity-Retaining Structures Using the Strength Reduction Method." *Journal of Geotechnical and Geoenvironmental Engineering* 150 (12). https://doi.org/10.1061/JGGEFK.GTENG-12209.

Tubaldi, E., C. J. White, E. Patelli, S. A. Mitoulis, G. de Almeida, J. Brown, M. Cranston, et al. 2022. "Invited Perspectives: Challenges and Future Directions in Improving Bridge Flood Resilience." *Natural Hazards and Earth System Sciences* 22 (3): 795–812. https://doi.org/10.5194/nhess-22-795-2022

Uray, E., S. Çarbaş, İH Erkan, and M. Olgun. 2020. "Investigation of Optimal Designs for Concrete Cantilever Retaining Walls in Different Soils." *Challenge Journal of Concrete Research Letters* 11 (2): 39. https://doi.org/10.20528/cjcrl.2020.02.003.

Vesić, A. S. 1973. "Analysis of Ultimate Loads of Shallow Foundations." *Journal of the Soil Mechanics and Foundations Division* 99 (1): 45–73. https://doi.org/10.1061/JSFEAQ.0001846

Appendix A. Earth pressures for cantilever walls adjacent to the river and under scour actions

A1.1. Active thrust

Figure A1 shows an ideal model of a retaining wall and the location of active pressure, which is assumed to be applied at the edge of the heel.

The horizontal and vertical components of active thrust are calculated by integrating the horizontal total stress σ_x and the tangential stress τ_{xz}, respectively, along the height H of the wall.

$$S_{ah} = \int_0^H (\sigma_x' + u_w)dz = \frac{1}{2}k_a\gamma H^2 + \frac{1}{2}(1-k_a)\gamma_w(H_w + D_F)^2 \quad \text{(A1)}$$

$$S_{av} = \int_0^H \tau_{xz}dz = \int_0^H k_a^*\sigma_z' dz = \frac{1}{2}k_a^*\gamma H^2 - \frac{1}{2}k_a^*\gamma_w(H_w + D_F)^2 \quad \text{(A2)}$$

$$k_a = \frac{\cos\delta}{1+\sin\phi'}\left(\cos\delta - \sqrt{\sin^2\phi' - \sin^2\delta}\right)e^{-2\theta\tan\phi'} \quad \text{(A3)}$$

$$k_a^* = \tan\delta k_a \quad \text{(A4)}$$

$$2\theta = \text{asin}\left(\frac{\sin\delta}{\sin\phi'}\right) - \delta \quad \text{(A5)}$$

$$u_w = \gamma_w[z - (H - (H_w + D_F))] \quad \text{(A6)}$$

A1.2. Passive thrust

Figure A2 shows the retaining wall and the location of passive pressure, which is assumed to be applied at the edge of the toe.

The horizontal and vertical components of passive thrust are calculated by integrating the horizontal total stress σ_x and the tangential stress τ_{xz}, respectively, along the embedded depth and the height of water.

$$S_{ph} = \int_0^{D_F} \sigma_x dz = \frac{1}{2}(\gamma - \gamma_w)k_p D_F^2 + \left(\frac{1}{2}\gamma_w D_F^2 + \gamma_w H_w D_F\right) \quad \text{(A7)}$$

$$S_{pv} = \int_0^{D_F} \tau_{xz}dz = \int_0^{D_F} k_p^*(\sigma_z - u_w)dz = \frac{1}{2}(\gamma - \gamma_w)k_p^* D_F^2 \quad \text{(A8)}$$

$$k_p = \frac{\cos\delta}{1-\sin\phi'}\left(\cos\delta + \sqrt{\sin^2\phi' - \sin^2\delta}\right)e^{2\theta\tan\phi'} \quad \text{(A9)}$$

$$k_p^* = \tan\delta k_p \quad \text{(A10)}$$

$$2\theta = \text{asin}\left(\frac{\sin\delta}{\sin\phi'}\right) + \delta \quad \text{(A11)}$$

$$u_w = \gamma_w(H_w + z) \quad \text{(A12)}$$

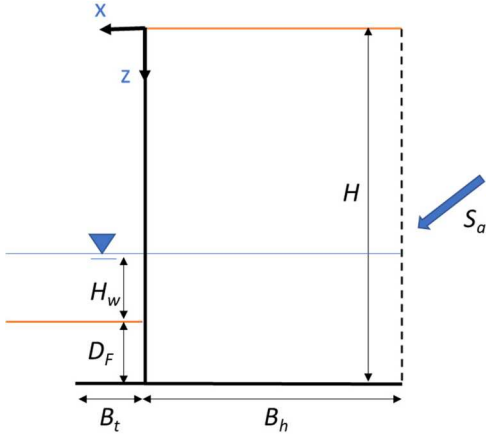

Figure A1. Ideal model for the active pressure of the retaining wall adjacent to the river

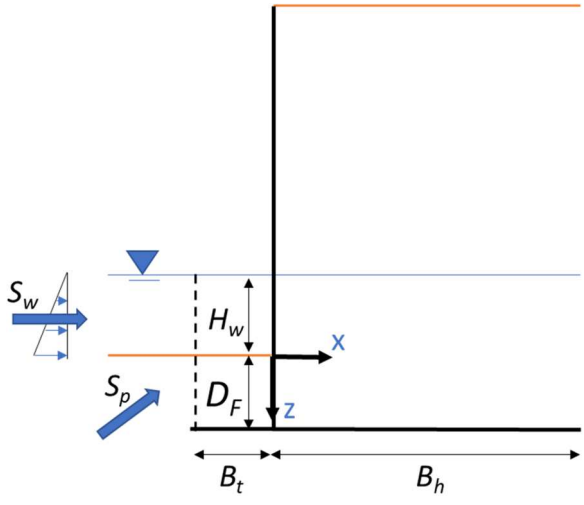

Figure A2. Ideal model for passive pressure of retaining wall adjacent to the river.

Appendix B. Overturning failure of retaining wall under progressive scour

For $D_T \leq D_F$, the overturning point is at the edge of the toe on the water side, and the overturning factor is given by:

$$f_{ov} = \frac{S_{ah,1}\frac{H}{3} + S_{ah,2}\frac{H_w + D_F}{3} + U\frac{B_t + B_h}{2}}{S_{av}(B_h + B_t) + W_h\left(\frac{B_h}{2} + B_t\right) + W_t\left(\frac{B_t}{2}\right) + S_w\left(\frac{H_w + D_T}{3} + D_F^{'}\right) + S_{ph,1}\frac{D_F^{'}}{3} + S_{ph,2}\frac{D_F^{'}}{2}} \tag{B1}$$

When $D_T > D_F$ and $0 < W_s \leq B_t/2$, the foundation is exposed, and the passive pressure is zero. The overturning point moves towards the heel but does not exceed the centre of the toe. This shift changes the overturning arm for active pressure, buoyancy force and the vertical resultant forces on the wall base. The expression of the overturning factor becomes:

$$f_{ov} = \frac{S_{ah,1}\frac{H}{3} + S_{ah,2}\frac{H_w + D_F}{3} + U\left|W_s - \frac{B_t + B_h}{2}\right|}{S_{av}|B_h + B_t - W_s| + W_h\left|\frac{B_h}{2} + B_t - W_s\right| + W_t\left|\frac{B_t}{2} - W_s\right| + S_w\left(\frac{H_w + D_F}{3}\right)} \tag{B2}$$

When $D_T > D_F$ and $B_t/2 < W_s \leq B_t/2 + B_h/2$, the overturning point moves further toward the heel, causing W_t to act as a destabilising force. The overturning factor is:

$$f_{ov} = \frac{S_{ah,1}\frac{H}{3} + S_{ah,2}\frac{H_w + D_F}{3} + W_t\left|\frac{B_t}{2} - W_s\right| + U\left|W_s - \frac{B_t + B_h}{2}\right|}{S_{av}|B_h + B_t - W_s| + W_h\left|\frac{B_h}{2} + B_t - W_s\right| + S_w\left(\frac{H_w + D_F}{3}\right)} \tag{B3}$$

When $D_T > D_F$ and $(B_t + B_h)/2 \leq W_s < B_t + B_h/2$, the overturning point moves beyond the centre of the foundation, causing the buoyancy to act as a stabilisation force. Thus, the overturning factor is given by:

$$f_{ov} = \frac{S_{ah,1}\frac{H}{3} + S_{ah,2}\frac{H_w + D_F}{3} + W_t\left|\frac{B_t}{2} - W_s\right|}{S_{av}|B_h + B_t - W_s| + W_h\left|\frac{B_h}{2} + B_t - W_s\right| + S_w\left(\frac{H_w + D_F}{3}\right) + U\left|W_s - \frac{B_t + B_h}{2}\right|} \tag{B4}$$

Finally, when $D_T > D_F$ and $W_s \geq B_t + B_h/2$, the overturning point moves beyond the centre of the heel, and W_h becomes a destabilising force.

$$f_{ov} = \frac{S_{ah,1}\frac{H}{3} + S_{ah,2}\frac{H_w + D_F}{3} + W_t\left|\frac{B_t}{2} - W_s\right| + W_h\left|\frac{B_h}{2} + B_t - W_s\right|}{S_{av}|B_h + B_t - W_s| + S_w\left(\frac{H_w + D_F}{3}\right) + U\left|W_s - \frac{B_t + B_h}{2}\right|} \tag{B5}$$